

Supporting Information

Strong Intermolecular Antiferromagnetic Verdazyl-Verdazyl Coupling in the Solid State

S. Eusterwiemann,^{a,†} C. Doerenkamp,^{b,†} T. Dresselhaus,^{a,c,†} O. Janka,^d M. de Oliveira Jr.,^e C. G. Daniliuc,^a H. Eckert,^{b,e} J. Neugebauer,^{a,c} R. Pöttgen^d and A. Studer^a

^{a.} *Institute of Organic Chemistry, Westfälische Wilhelms-Universität Münster, Corrensstrasse 40, 48149 Münster, Germany. E-Mail: studer@uni-muenster.de*

^{b.} *Institute of Physical Chemistry, Westfälische Wilhelms-Universität Münster, Corrensstrasse 28/30, 48149 Münster, Germany. E-Mail: eckerth@uni-muenster.de*

^{c.} *Center for Multiscale Theory and Computations, Westfälische Wilhelms-Universität Münster, Corrensstrasse 40, 48149 Münster, Germany. E-Mail: j.neugebauer@uni-muenster.de*

^{d.} *Institute of Inorganic and Analytical Chemistry, Westfälische Wilhelms-Universität Münster, Corrensstrasse 28/30, 48149 Münster, Germany. E-Mail: pottgen@uni-muenster.de*

^{e.} *Instituto de Física de São Carlos, Universidade de São Paulo, São Carlos, São Paulo 13560-970, Brazil. E-Mail: eckerth@uni-muenster.de*

† equally contributing authors.

Table of Contents

1. General Information.....	3
2. Experimental Data	5
3. X-Ray Crystal Structure Analysis	7
4. Absorption Spectra	10
5. EPR Spectra	11
6. Cyclic Voltammetry Measurements	14
7. Physical Properties.....	15
8. Comparison of T-dependent Magnetic Susceptibilities Measured via Magnetic Force Detection and EPR Intensity	16
9. Quantum Chemical Calculations	17
10. Solid-State NMR Spectroscopy	20
11. ^1H and ^{13}C NMR Spectra.....	21
12. References.....	23

1. General Information

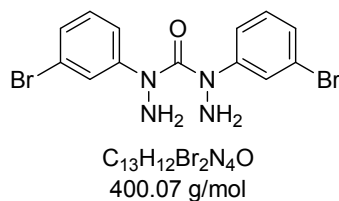
Liquid state ^1H NMR and ^{13}C NMR spectra were recorded on a *Bruker DPX 300*, a *Bruker AV 300* or a *Bruker AV 400* spectrometer at room temperature (rt). The chemical shifts were referred to the solvent residual peak (CDCl_3 : ^1H : δ 7.26 ppm, ^{13}C : δ 77.16 ppm; $\text{DMSO-}d_6$: ^1H : δ 2.50 ppm, ^{13}C : δ 39.52 ppm; C_6D_6 : ^1H : δ 7.16 ppm). Multiplicities of NMR signals are described as *s* (singlet), *d* (doublet), *t* (triplet) or *m* (multiplet). **Solid state ^1H NMR** and ^{13}C NMR spectra were recorded on a *Bruker DSX 400* NMR spectrometer with a 4 mm double resonance NMR probe. The resonance frequencies were 100.7 MHz for ^{13}C and 400.0 MHz for ^1H at 9.4 Tesla. Chemical shifts are reported using adamantane (^1H : 1.78 ppm) (^{13}C : 38.56 ppm for the methane resonance) as secondary reference. ^1H MAS-NMR spectra were recorded by means of rotor-synchronized Hahn echo experiments at a spinning frequency of 15 kHz. The 90° pulse length was 4 μs , and a recycle delay of 1 s was used. ^{13}C spectra were measured by proton decoupled EASY sequence at a spinning frequency of 10 and 15 kHz and ramped $^{13}\text{C}\{^1\text{H}\}$ CP/MAS at a spinning frequency of 10 kHz, with typical 90° pulse lengths of 5.0 μs , TPPM-15 proton decoupled acquisition and recycle delays of <1s. Contact times of 50 μs . were used. **Mass spectra** (HRMS - ESI) were recorded on a *Finnigan MAT 4200S*, *Bruker Daltonics Micro-TOF*, a *Micromass Quatro LCZ* (ESI) or a *Bruker LTQ Orbitrap XL* and peaks are given in *m/z*. **IR spectra** were recorded on a *Digilab Varian 3100 FT-IR Excalibur Series* equipped with a MKII Golden Gate Single Reflection ATR unit. Recorded IR signals are reported in wavelength (cm^{-1}) with the following abbreviation for the intensity of absorption: *s* = strong, *m* = medium, *w* = weak. **Melting points** (M.p.) were measured on a *Stuart SMP-10* melting point apparatus and are uncorrected. **Elemental analysis** was performed at a *Vario EL III* of the company *Elementar-Analysensysteme GmbH*. **UV/Vis spectra** were measured at rt in CH_2Cl_2 (\sim 0.83 mM) in a quartz cuvette (0.1 mm QS) with a *Varian Cary 1Bio*. **Liquid state EPR measurements** were carried out at room temperature on 1 mM solutions in CH_2Cl_2 (purged with nitrogen) on an E-580 *Bruker* ELEXSYS X-band EPR spectrometer (9.48 GHz). 1024 data points at a centre field of 348.5 mT, a sweep width of 9 mT and a sweep time of 83.9 s were recorded. Field modulation amplitudes and frequency were 0.1 mT and 100 kHz respectively. The microwave power attenuation level was 32db. **Solid state EPR measurements** were carried out in continuous-wave mode on a E-580 *Bruker* ELEXSYS X-band EPR spectrometer equipped with an Oxford cryogenic system. For the acquisition of the spectra the following parameters were used: Microwave power attenuation level 35 dB, sweep rate 1.1 G/s, sweep width 90 G, modulation frequency and amplitude 100 kHz and 1 G, respectively. **Thin layer chromatography** (TLC)

was carried out on *Merck* silica gel 60 F254 plates; detection by UV (irradiation at 254 nm) or dipping into a solution of KMnO_4 (1.5 g), NaHCO_3 (5.0 g) in H_2O (400 mL), followed by heating. **Flash chromatography** (FC) was performed on silica gel (*Merck*-Si 60: 40–63 μm) with a pressure of 0.1 to 0.5 bar. Used eluents are given in parentheses. **Solvents:** All solvents for extraction and FC were distilled before use. **Magnetic Properties:** A powdered sample of the verdazyl radical was filled in a PE capsule and attached to the sample holder rod of a Vibrating Sample Magnetometer (VSM) unit for measuring the magnetization $M(T,H)$ in a Quantum Design Physical-Property-Measurement-System (PPMS). The sample was investigated in the temperature range of 2.5–350 K and with magnetic flux densities up to 80 kOe. **Heat Capacity:** For the heat capacity measurement, one piece of the sample was fixed to a pre-calibrated heat capacity puck using Apiezon N grease and investigated in the temperature range of 2.0–250 K.

Techniques: All reactions involving air or moisture sensitive reagents or intermediates were carried out under argon atmosphere using standard *Schlenk* techniques. All glasswares were dried by the use of a heat gun under high vacuum prior to use. Concentration of the reaction mixture was performed under reduced pressure at 40 °C at the appropriate pressure. Purified compounds were further dried under high vacuum. All **reagents** were purchased of the following companies and have been used without further purification: *Acros Organics*, *Sigma-Aldrich*, *Alfa Aesar*, *TCI Germany* or *Merck*.

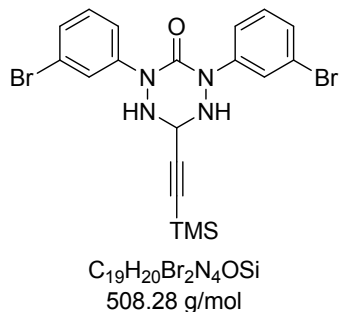
2. Experimental Data

N,N'-Bis-(3-bromophenyl)carbonohydrazide (**S1**)



According to a literature procedure^{1, 2} in a sealed tube CuI (105 mg, 554 μ mol, 5 mol%), 1,10-phenanthroline (200 mg, 1.11 mmol, 10 mol%), K_3PO_4 (7.178 g, 33.82 mmol, 3.05 equiv.) and carbonohydrazide (1.00 g, 11.1 mmol, 1.0 equiv.) were added, evacuated and backfilled with Argon two consecutive times. Then 1-bromo-3-iodobenzene (3.26 mL, 25.5 mmol, 2.3 equiv.) and DMF (22 mL) were added and the mixture was heated to 90 °C and stirred for 48 h at this temperature. After the reaction mixture was allowed to cool to rt it was filtered through a short pad of silica and eluted with EtOAc. Water (30 mL) was added and the two layers were separated. The aqueous layer was extracted with EtOAc (2 \times 40 mL) and the combined organic layers were washed with brine and dried over $MgSO_4$. Filtration, evaporation of the solvent *in vacuo* and FC (*n*-pentane/MTBE 1:10) afforded the title compound (1.59 g, 3.97 mmol, 36%) as an orange oil. **IR** (ATR, neat): 3337w, 2251w, 1728w, 1657m, 1624m, 1587m, 1571m, 1474m, 1428w, 1337m, 1252m, 1089w, 1070w, 1045w, 996w, 904s, 779w, 724s, 682m, 648m; **¹H NMR** (300 MHz, $CDCl_3$): δ 7.33-7.25 (m, 2H, CH_{arom}), 7.21-7.10 (m, 2H, CH_{arom}), 7.07-7.03 (m, 2H, CH_{arom}), 4.28 (s, 4H, 2 \times NH_2); **¹³C NMR** (75 MHz, $CDCl_3$): δ 145.5 (C), 130.0 (2 \times CH), 128.4 (2 \times CH), 126.7 (2 \times CH), 126.0 (2 \times C), 122.3 (2 \times C), 122.0 (2 \times CH); **HRMS** (ESI): m/z = 398.9451 calcd. for $[M+H]^+$ and 420.9270 calcd. for $[M+Na]^+$, found: 398.9453 and 420.9278.

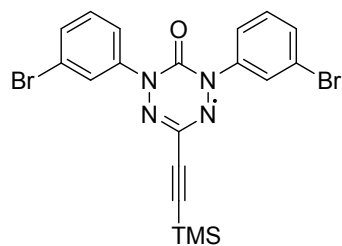
2,4-Bis(3-bromophenyl)-6-((trimethylsilyl)ethynyl)-1,2,4,5-tetrazinan-3-one (**S2**)



In a two-necked flask with condenser compound **S1** (600 mg, 1.50 mmol, 1.0 equiv.) was dissolved in MeOH (4 mL) and stirred at 45 °C for 5 min. A solution of 3-(trimethylsilyl)-2-propynal (220 μ L, 1.50 mmol, 1.0 equiv.) in MeOH (3 mL) was added dropwise within 30 minutes. After addition the mixture was refluxed for 3.5 h. Stirring was stopped and the mixture was cooled down to rt. The precipitate was filtered off and washed carefully with little amounts of cold MeOH. The filtrate was cooled to -14 °C overnight and the achieved precipitate filtered off again and washed with cold MeOH. The combined solids were dried *in vacuo* to give the title compound (453 mg, 891 μ mol, 59%) as a colorless solid. **M.p.**: 159 °C; **IR** (ATR, neat): 3268w, 2960w, 1628s, 1587m, 1472m, 1420w,

1359s, 1252s, 1125w, 1971w, 1027w, 909m, 874m, 844s, 778s, 762m, 736m, 683s, 671m, 624w, 598m; **¹H NMR** (300 MHz, DMSO-*d*₆): δ 7.77 (*s*, 2H, 2 × CH_{arom}), 7.58 (*m*, 2H, 2 × CH_{arom}), 7.29 (*d*, *J* = 4.8 Hz, 4H, 4 × CH_{arom}), 6.54 (*d*, *J* = 6.1 Hz, 2H, 2 × NH), 5.20 (*t*, *J* = 5.9 Hz, 1H, CH), 0.13 (*s*, 9H, Si-CH₃); **¹³C NMR** (75 MHz, DMSO-*d*₆): δ 155.1 (C), 144.3 (2 × C), 129.8 (2 × CH), 126.3 (CH), 124.1 (2 × CH), 120.7 (2 × C), 120.6 (2 × CH), 101.5 (C), 89.7 (C), 62.0 (CH), -0.5 (3 × CH₃); **HRMS** (ESI): *m/z* = 506.9846 calcd. for [M+H]⁺ and 528.9665 calcd. for [M+Na]⁺, found: 506.9840 and 528.9647.

1,5-Bis(3-bromophenyl)-3-((trimethylsilyl)ethynyl)-6-oxo-verdazyl (1)



C₁₉H₁₇Br₂N₄OSi⁺
505.26 g/mol

In a reaction tube compound **S2** (161 mg, 317 μmol 1.0 equiv.) and 1,4-benzoquinone (58 mg, 0.54 mmol, 1.7 equiv.) were added and dissolved in CH₂Cl₂ (8 mL). The mixture was heated at 60 °C for 4 h. After cooling down to rt the solvent was removed *in vacuo* and the residue subjected to FC (*n*-pentane/MTBE 25:1), which gave the title compound (115 mg, 228 μmol, 75%) as a dark red solid. Single crystals suitable for X-Ray analysis were achieved by slow evaporation of a CHCl₃, MeCN or acetone solution at rt over several days. **M.p.:** 141 °C; **IR** (ATR, neat): 1721*m*, 1583*m*, 1473*m*, 1427*m*, 1381*w*, 1349*w*, 1250*m*, 1209*m*, 1132*w*, 939*w*, 844*s*, 777*s*, 760*m*, 726*s*, 707*m*, 679*s*, 654*s*, 634*w*, 614*s*; **HRMS** (ESI): *m/z* = 525.9431 calcd. for [M+Na]⁺, found: 525.9421; **Elemental analysis:** calcd. for C₁₉H₁₇N₄OBr₂Si: C, 45.17, H, 3.39, N, 11.09, found: C, 45.65, H, 3.44, N, 10.86.

3. X-Ray Crystal Structure Analysis

X-Ray diffraction: For compounds **1-(223K)** and **1-(173K)** data sets were collected with a Nonius Kappa CCD diffractometer. Programs used: data collection, COLLECTⁱ; data reduction Denzo-SMN³; absorption correction, Denzo⁴; structure solution SHELXS-97⁵; structure refinement SHELXL-97⁶ and graphics, XPⁱⁱ. For compound **1-(100K)** data sets were collected with a Bruker APEX II CCD diffractometer. For compound **1-(80K)** data sets were collected with a Bruker D8 Venture PHOTON 100 CMOS diffractometer. Programs used: data collection: APEX2 V2014.5-0ⁱⁱⁱ; cell refinement: SAINT V8.34A^{iv}; data reduction: SAINT V8.34A^{iv}; absorption correction, SADABS V2014/2ⁱⁱⁱ; structure solution SHELXT-2014^v; structure refinement SHELXL-2014^v and graphics, XPⁱⁱⁱ. *R*-values are given for observed reflections, and *wR*² values are given for all reflections.

X-ray crystal structure analysis of 1-(223K): formula C₁₉H₁₇Br₂N₄OSi, *M* = 505.28, red crystal, 0.13 x 0.10 x 0.03 mm, *a* = 7.1372(1), *b* = 10.9703(3), *c* = 13.9865(4) Å, α = 72.911(1), β = 86.154(1), γ = 86.504(2)°, *V* = 1043.4(1) Å³, ρ_{calc} = 1.61 gcm⁻³, μ = 4.0 mm⁻¹, empirical absorption correction (0.627 ≤ *T* ≤ 0.890), *Z* = 2, triclinic, space group *P* $\bar{1}$ (No. 2), λ = 0.71073 Å, *T* = 223(2) K, ω and ϕ scans, 9882 reflections collected ($\pm h, \pm k, \pm l$), 5111 independent (*R*_{int} = 0.042) and 4061 observed reflections [*I* > 2σ(*I*)], 247 refined parameters, *R*1 = 0.055, *wR*2 = 0.121, max. (min.) residual electron density 0.62 (-0.78) e.Å⁻³, hydrogen atoms were calculated and refined as riding atoms.

X-ray crystal structure analysis of 1-(173K): formula C₁₉H₁₇Br₂N₄OSi, *M* = 505.28, red crystal, 0.33 x 0.13 x 0.02 mm, *a* = 7.1059(5), *b* = 10.9332(8), *c* = 13.9604(11) Å, α = 72.976(3), β = 85.718(3), γ = 86.366(4)°, *V* = 1033.2(1) Å³, ρ_{calc} = 1.62 gcm⁻³, μ = 4.0 mm⁻¹, empirical absorption correction (0.352 ≤ *T* ≤ 0.779), *Z* = 2, triclinic, space group *P* $\bar{1}$ (No. 2), λ = 0.71073 Å, *T* = 173(2) K, ω and ϕ scans, 7790 reflections collected ($\pm h, \pm k, \pm l$), 3434 independent (*R*_{int} = 0.063) and 2929 observed reflections [*I* > 2σ(*I*)], 247 refined parameters, *R*1 = 0.062, *wR*2 = 0.169, max. (min.) residual electron density 0.83 (-0.96) e.Å⁻³, hydrogen atoms were calculated and refined as riding atoms.

ⁱ R. W. W. Hooft, Bruker AXS, **2008**, Delft, The Netherlands.

ⁱⁱ Bruker AXS, **2000**, Madison, Wisconsin, USA.

ⁱⁱⁱ APEX2, SADABS, Bruker AXS Inc., **2014**, Madison, Wisconsin, USA.

^{iv} SAINT, Bruker AXS Inc., **2013**, Madison, Wisconsin, USA.

^v Sheldrick, **2014**.

X-ray crystal structure analysis of 1-(100K): A dark red plate-like specimen of $C_{19}H_{17}Br_2N_4OSi$, approximate dimensions 0.020 mm x 0.100 mm x 0.240 mm, was used for the X-ray crystallographic analysis. The X-ray intensity data were measured. A total of 1716 frames were collected. The total exposure time was 37.91 hours. The frames were integrated with the Bruker SAINT software package using a wide-frame algorithm. The integration of the data using a triclinic unit cell yielded a total of 17434 reflections to a maximum θ angle of 66.70° (0.84 Å resolution), of which 3572 were independent (average redundancy 4.881, completeness = 99.5%, $R_{int} = 7.98\%$, $R_{sig} = 3.93\%$) and 3436 (96.19%) were greater than $2\sigma(F^2)$. The final cell constants of $a = 7.0581(2)$, $b = 10.8956(3)$, $c = 13.8636(4)$ Å, $\alpha = 73.1680(10)$, $\beta = 85.1820(10)$, $\gamma = 86.3520(10)^\circ$, volume = $1016.00(5)$ Å³, are based upon the refinement of the XYZ-centroids of 9947 reflections above $20\sigma(I)$ with $6.676^\circ < 2\theta < 133.1^\circ$. Data were corrected for absorption effects using the multi-scan method (SADABS). The ratio of minimum to maximum apparent transmission was 0.651. The calculated minimum and maximum transmission coefficients (based on crystal size) are 0.338 and 0.893. The final anisotropic full-matrix least-squares refinement on F^2 with 247 variables converged at $R1 = 3.59\%$, for the observed data and $wR2 = 8.69\%$ for all data. The goodness-of-fit was 1.091. The largest peak in the final difference electron density synthesis was $0.92 e^-/\text{Å}^3$ and the largest hole was $-0.44 e^-/\text{Å}^3$ with an RMS deviation of $0.098 e^-/\text{Å}^3$. On the basis of the final model, the calculated density was 1.65 g/cm^3 and $F(000)$, 502 e^- .

X-ray crystal structure analysis of 1-(80K): A dark red prism-like specimen of $C_{19}H_{17}Br_2N_4OSi$, approximate dimensions 0.090 mm x 0.145 mm x 0.346 mm, was used for the X-ray crystallographic analysis. The X-ray intensity data were measured. A total of 464 frames were collected. The total exposure time was 2.58 hours. The frames were integrated with the Bruker SAINT software package using a narrow-frame algorithm. The integration of the data using a triclinic unit cell yielded a total of 18645 reflections to a maximum θ angle of 27.53° (0.77 Å resolution), of which 4658 were independent (average redundancy 4.003, completeness = 99.4%, $R_{int} = 3.19\%$, $R_{sig} = 2.62\%$) and 4072 (87.42%) were greater than $2\sigma(F^2)$. The final cell constants of $a = 7.0548(3)$, $b = 10.8999(4)$, $c = 13.8588(5)$ Å, $\alpha = 73.194(2)$, $\beta = 85.0620(10)$, $\gamma = 86.312(2)^\circ$, volume = $1015.52(7)$ Å³, are based upon the refinement of the XYZ-centroids of 9898 reflections above $20\sigma(I)$ with $5.622^\circ < 2\theta < 55.01^\circ$. Data were corrected for absorption effects using the multi-scan method (SADABS). The ratio of minimum to maximum apparent transmission was 0.863. The calculated minimum and maximum transmission coefficients (based on crystal size) are 0.334 and 0.711. The final anisotropic full-matrix least-squares refinement on F^2 with 247 variables converged at $R1 = 2.13\%$, for the observed data and $wR2 = 4.85\%$ for all data. The goodness-of-

fit was 1.042. The largest peak in the final difference electron density synthesis was $0.36 \text{ e}/\text{\AA}^3$ and the largest hole was $-0.45 \text{ e}/\text{\AA}^3$ with an RMS deviation of $0.070 \text{ e}/\text{\AA}^3$. On the basis of the final model, the calculated density was $1.65 \text{ g}/\text{cm}^3$ and $F(000)$, 502 e^- .

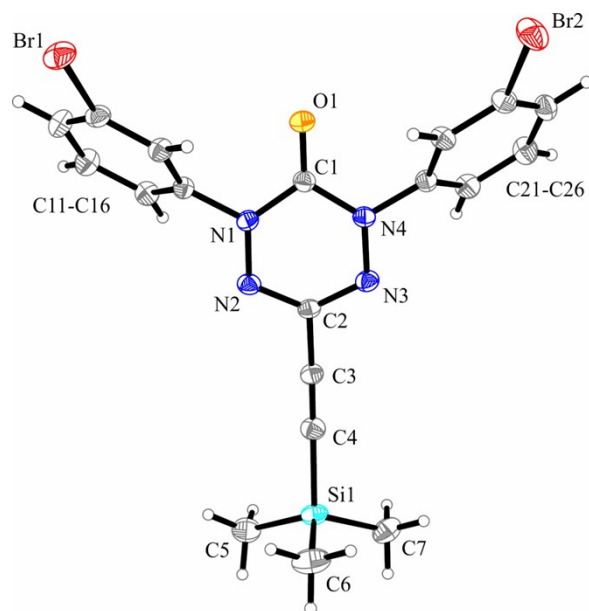


Figure S1. Molecular entity in the crystal structure of verdazyl radical **1-(223K)**. Displacement ellipsoids are shown with 30% probability.

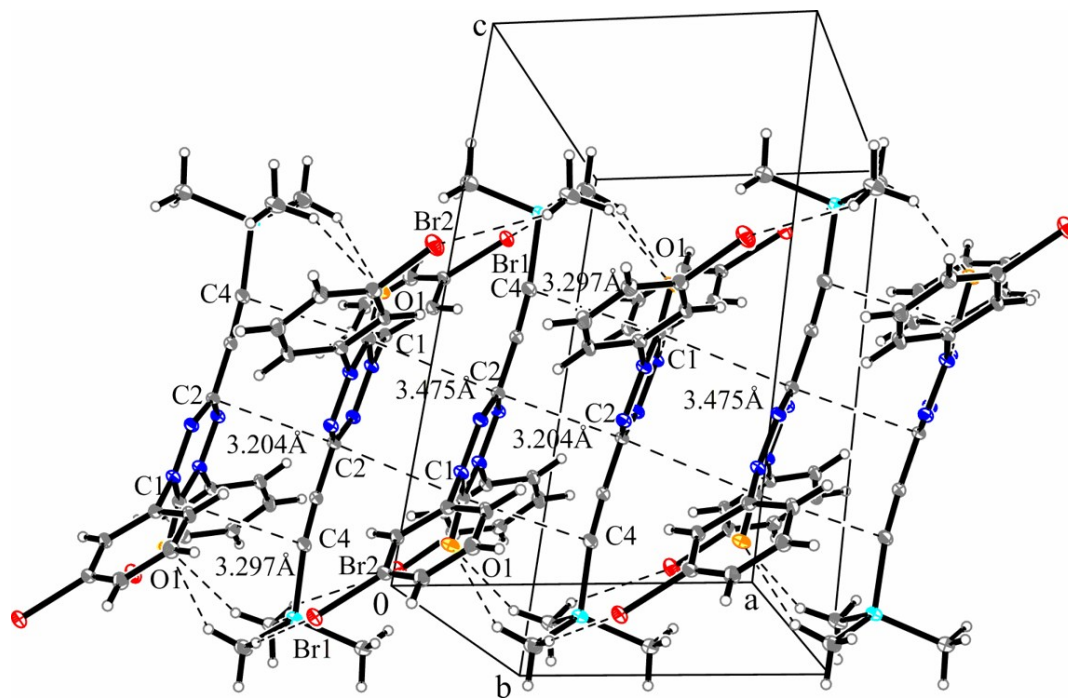


Figure S2. Extended unit cell showing the $\pi \cdots \pi$, $X\text{-H} \cdots O$ and $C\text{-H} \cdots Br$ interactions along the a -axis in solid **1-(223 K)**.

4. Absorption Spectra

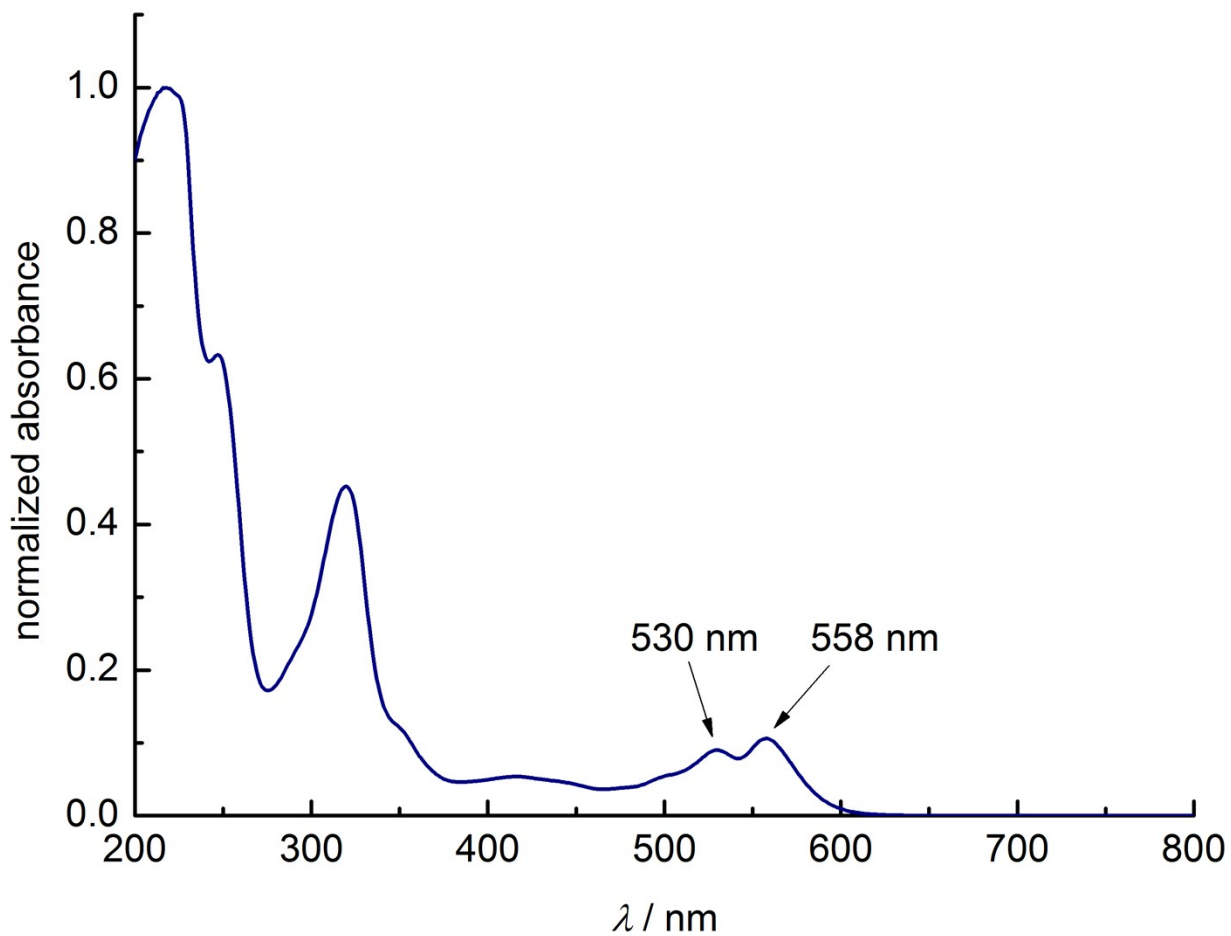


Figure S3. Absorption spectrum of verdazyl radical **1** in CH_2Cl_2 (0.08 mM) at rt.

5. EPR Spectra

a) Liquid State:

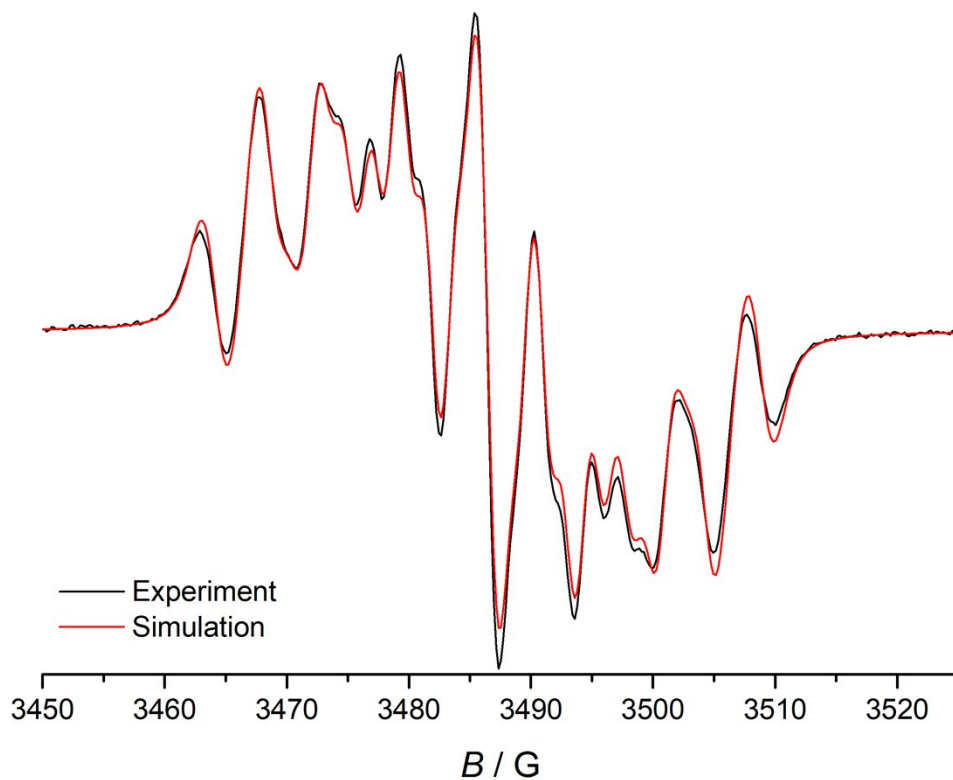


Figure S4. Liquid state EPR spectrum of verdazyl radical **1** in degassed dichloromethane at rt (black = experimental spectrum, red = simulation). Recorded at 9.78 GHz on a X-band Bruker ELEXSYS EPR spectrometer. The modulation amplitude used was 1 Gauss.

Table S1: Summary of the simulated A_{iso} values (in Gauss) and g -value, shown in Fig. S4.

g value	A_1 (N-1,5) / G	A_2 (N-2,4) / G	A_3 (H _{ortho}) / G	A_4 (H _{meta}) / G	A_5 (H _{para}) / G
2.0037	4.55	6.60	0.65	0.53	0.40

b) Solid State:

Figure S5a shows solid-state EPR spectra at different temperatures. In order to better show how the EPR intensities evolve with temperature, Figure S5b shows the first integral of the EPR spectra as a function of temperature. The evolution of the spectral lineshapes with temperature can be observed by the set of normalized spectra shown in Figure S6a and by their respective peak-to-peak widths, shown as a function of temperature in Figure S6b. The residual broad signal might be due to an impurity or due to some isolated spins in defect sites that are not involved in dimer formation (frustration). Because these species are relatively isolated, a structured spectrum defined by g -anisotropy and anisotropic hyperfine coupling is observed.

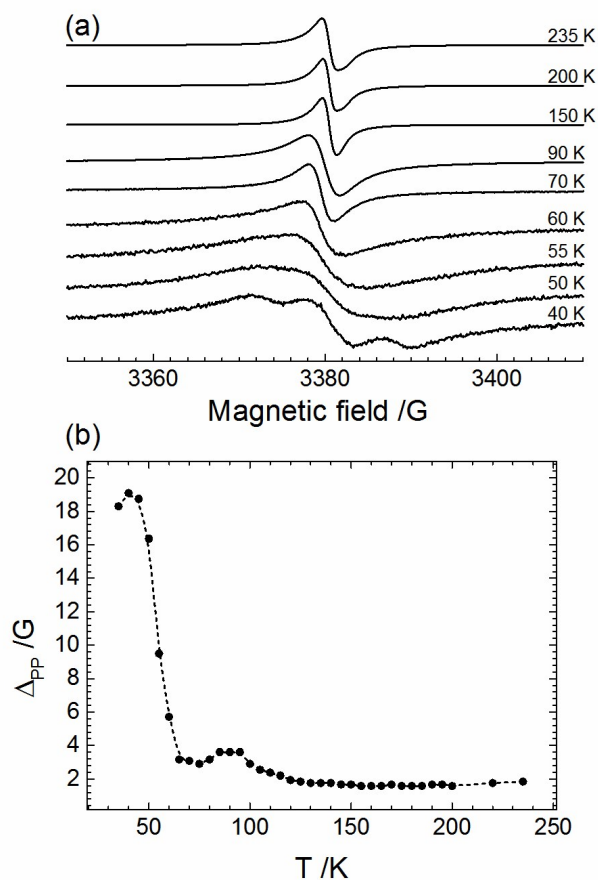


Figure S5. (a) Normalized EPR spectra for verdazyl radical **1** at selected temperatures. (b) EPR spectral peak-to-peak linewidths (Δ_{pp}) as a function of temperature.

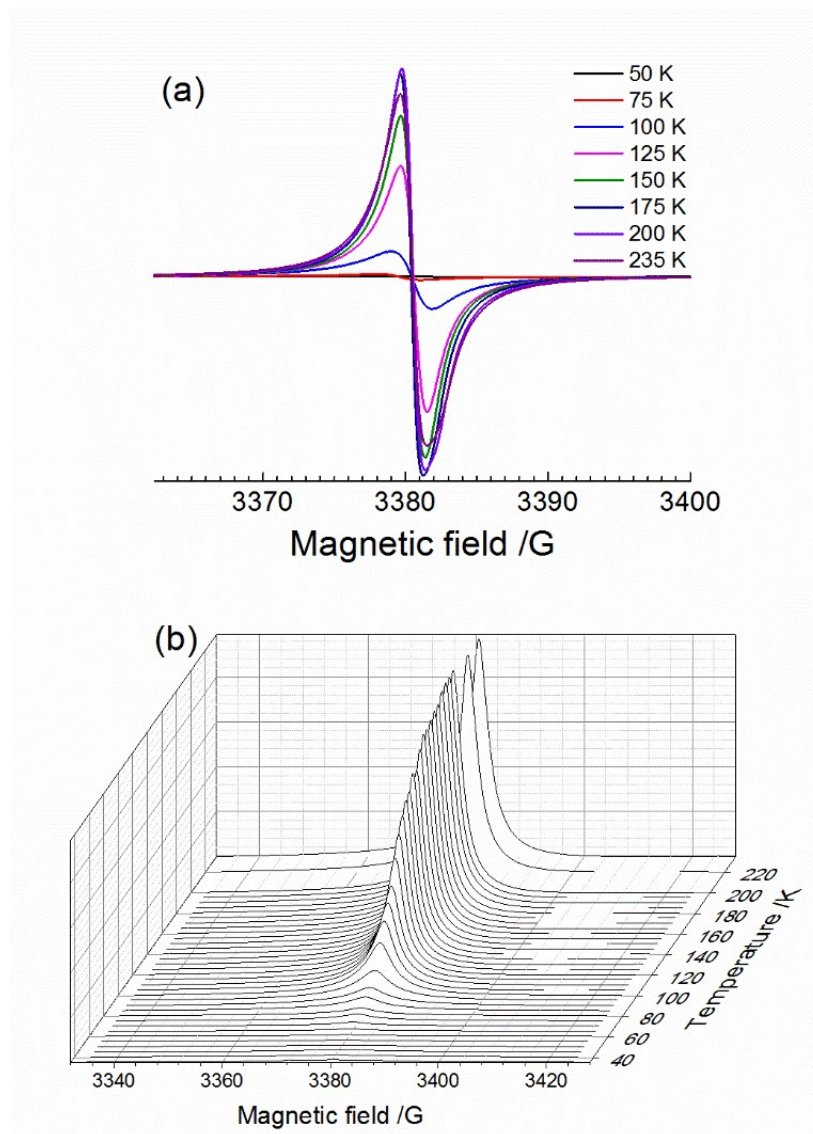


Figure S6. (a) Experimental EPR spectra for verdazyl radical **1** at selected temperatures. (b) Plot of the integrated EPR spectra for the whole temperature range investigated.

6. Cyclic Voltammetry Measurements

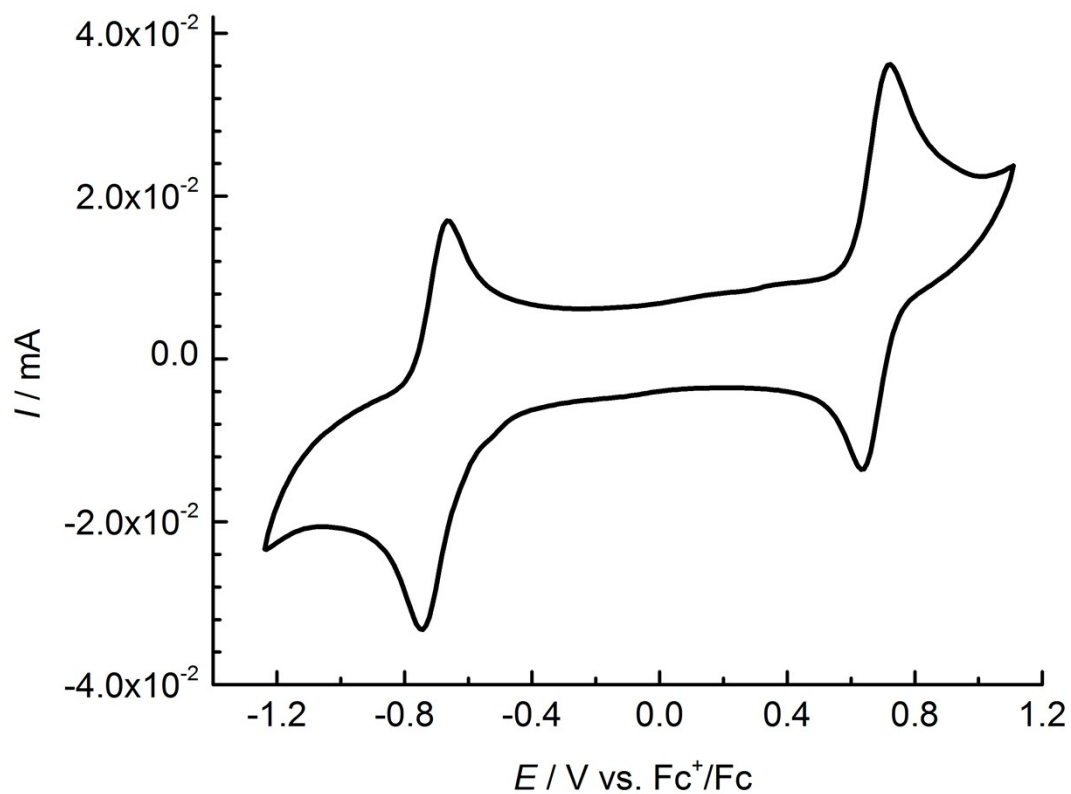


Figure S7. Cyclic voltammetry measurement of verdazyl radical **1** in MeCN with *n*-butylammonium tetrafluoroborate as an electrolyte, measured against ferrocene as an internal standard (scan rate = 0.1 V s^{-1}).

7. Physical Properties

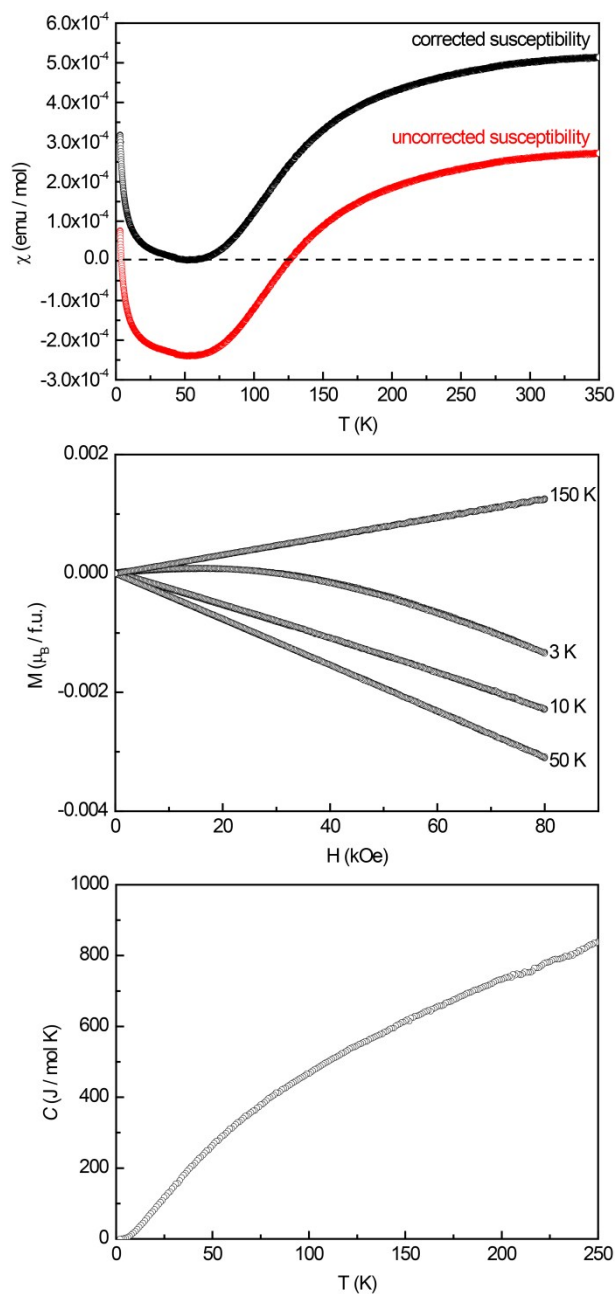


Figure S8. (top) Measurements of the temperature dependent magnetic susceptibilities at 10 kOe for verdazyl radical **1** from 2.5 K to 350 K. The uncorrected susceptibility is depicted in red, the paramagnetic susceptibility determined by subtracting the diamagnetic contribution (estimated using the Pascal constants) is plotted in black; (middle) magnetization isotherms recorded at 3, 10, 50 and 150 K; (bottom) heat capacity measurement of **1**. No phase transition is visible in the temperature range from 2 to 250 K.

8. Comparison of T-dependent Magnetic Susceptibilities Measured via Magnetic Force Detection and EPR Intensity

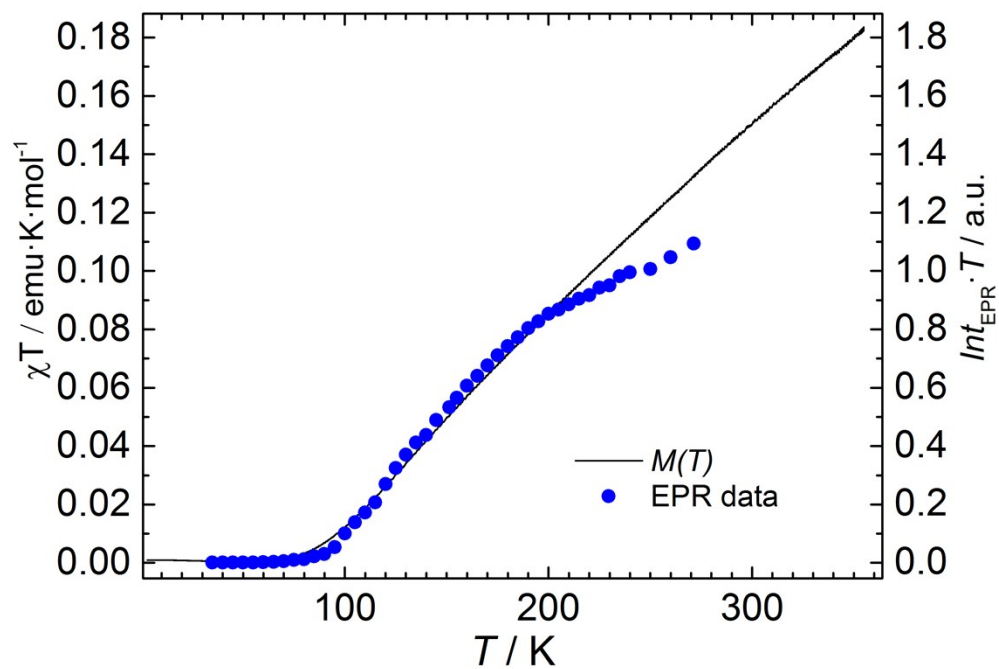


Figure S9. Temperature dependence of the product of the magnetic susceptibility and temperature, χT obtained from magnetic force detection and EPR signal intensity measurements for verdazyl radical **1**.

9. Quantum Chemical Calculations

Quantum chemical calculations have been performed according to the procedure described in the Reference 7. This procedure closely follows the *first-principles bottom-up* approach^{7, 8}, assuming a Heisenberg Hamiltonian,

$$\hat{H} = -2 \sum_{i < j} J_{ij} \hat{S}_i \hat{S}_j,$$

in which pairs of local spins \hat{S}_i on sites i interact with each other with a coupling constant J , all symmetry-unique interacting pairs of radical molecules inside a crystal structure are identified. For each pair a coupling constant is calculated with the broken symmetry formalism⁹ by employing ORCA¹⁰ with the PBE0 functional¹¹ in a ma-Def2-TZVP basis set¹². Based on the network set up by the relevant coupling constants, a magnetic unit cell is identified and extended along the directions into which the system shows a magnetic periodicity. For the resulting magnetic model, the Heisenberg Hamiltonian is set up and diagonalized. By assuming a Boltzmann distribution, the magnetic susceptibility and magnetic heat capacity can be calculated for each model.

For the studied system only two coupling constants have been found to be relevant. The values for the structures obtained at different temperatures are given in Table 1 of the main article. Other couplings (for the structure obtained at 223 K: $J_3 = -0.4 \text{ cm}^{-1}$, $J_4 = -0.1 \text{ cm}^{-1}$) are several orders of magnitude smaller and did not influence the results notably. Thus, the resulting model corresponds to a Heisenberg chain with alternating couplings J_1 and J_2 . In Figure S11, the magnetic susceptibilities obtained for models based on the coupling constants at different temperatures are shown. A model size of six cells along the a -axis (corresponding to 12 magnetic sites) has been used. To assess the quality of convergence, simulation results for smaller models comprising five or four cells, respectively, are shown for the 223 K structure. Clearly, the results are well converged as these curves are nearly indistinguishable. The magnetic heat capacity resulting from the discussed models is shown in Figure S12.

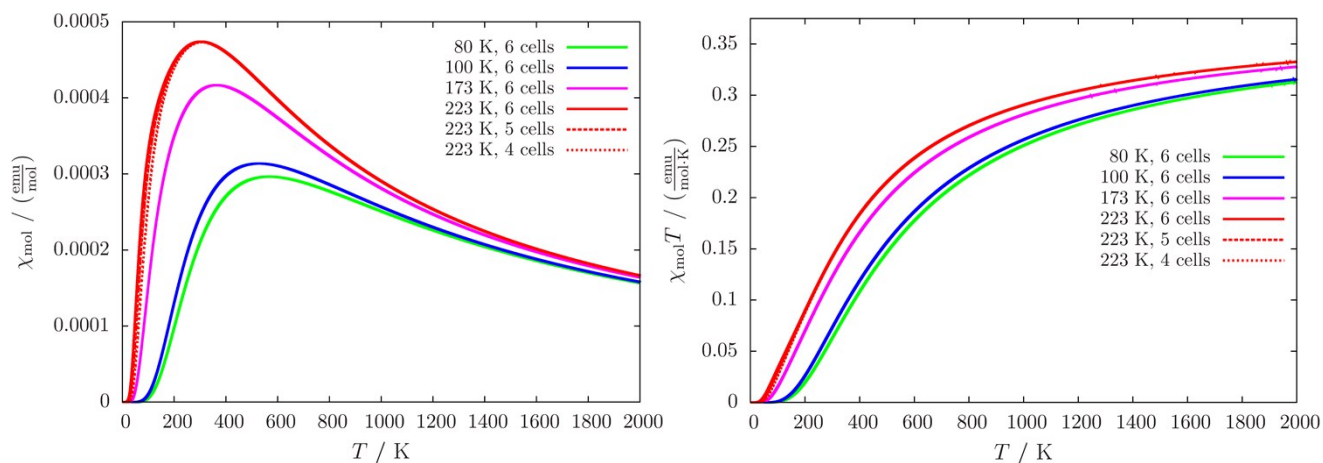


Figure S10. The predicted magnetic susceptibility for the studied verdazyl radical **1** based on the structures and coupling constants at different temperatures, plotted as molar susceptibility *versus* temperature (left) and as molar susceptibility times temperature *versus* temperature (right).

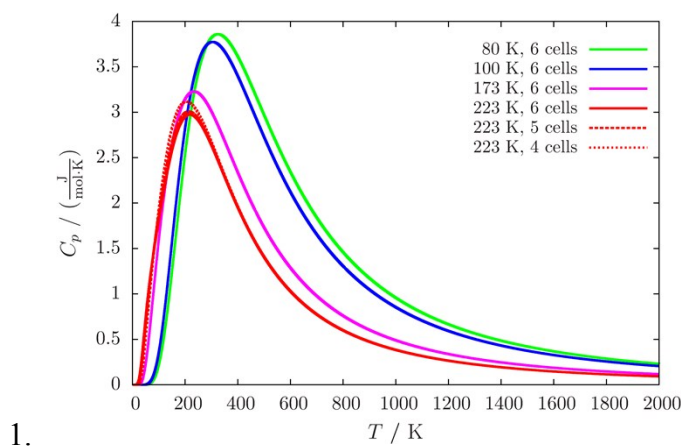


Figure S11. The predicted magnetic heat capacity for the studied verdazyl radical **1** based on the structures and coupling constants at different temperatures.

To further prove the validity of our results, we calculated the *closed-shell* singlet state as well. For this test we chose to look at the molecule pair with the strongest interactions, which is at the same time the molecule pair with the smallest intermolecular distance: the one responsible for J_1 in the structure obtained at 80 K. The closed-shell singlet state was 24.9 mE_H (corresponding to 5465 cm⁻¹) higher in energy than the broken-symmetry state and thus much higher in energy than the triplet state in our DFT calculations.

(For comparison: the energy of the triplet state was 335 cm^{-1} higher in energy than the broken-symmetry state.)

We also performed a CASSCF calculation on that system, where only the two magnetic orbitals were active and orbitals were optimized with averaging over the triplet and two singlet states. The state with lowest energy was a singlet state with 97 % weight of the open-shell configuration state function. The triplet state was 512 cm^{-1} higher in energy and the closed-shell singlet state 29946 cm^{-1} higher. In an additional NEVPT2¹³ calculation to correct for dynamic correlation effects, the triplet state was 666 cm^{-1} higher, and the closed-shell singlet state 21969 cm^{-1} higher in energy than the open-shell singlet state. Thus, the qualitative results of the DFT calculations could clearly be confirmed.

For the calculation of spin populations a single molecule has been extracted from the crystal structure and its geometry has been further optimized with ORCA¹⁰ using the TPSS functional¹⁴ in a Def2-TZVP basis set¹⁵ within the resolution-of-the-identity approximation¹⁶ and using dispersion correction¹⁷. Mulliken spin populations¹⁸ have been obtained for the optimized geometry employing the PBE0 functional¹¹ in the same basis. For comparison, Bader spin populations¹⁹ have been calculated with ADF²⁰ using the PBE0 functional¹¹ in a TZ2P basis²¹. The results are shown in Figure S13.

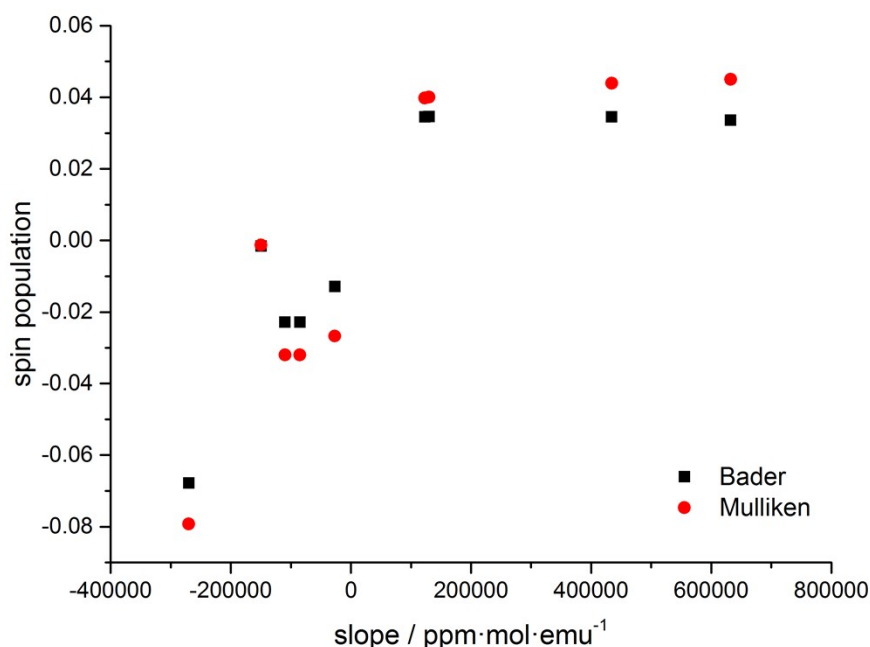


Figure S12. Comparison between calculated Bader and Mulliken spin populations and the slopes observed for the temperature dependent shifts which correlate with the paramagnetic contributions to the magnetic susceptibilities observed in Figure 5.

10. Solid-State NMR Spectroscopy

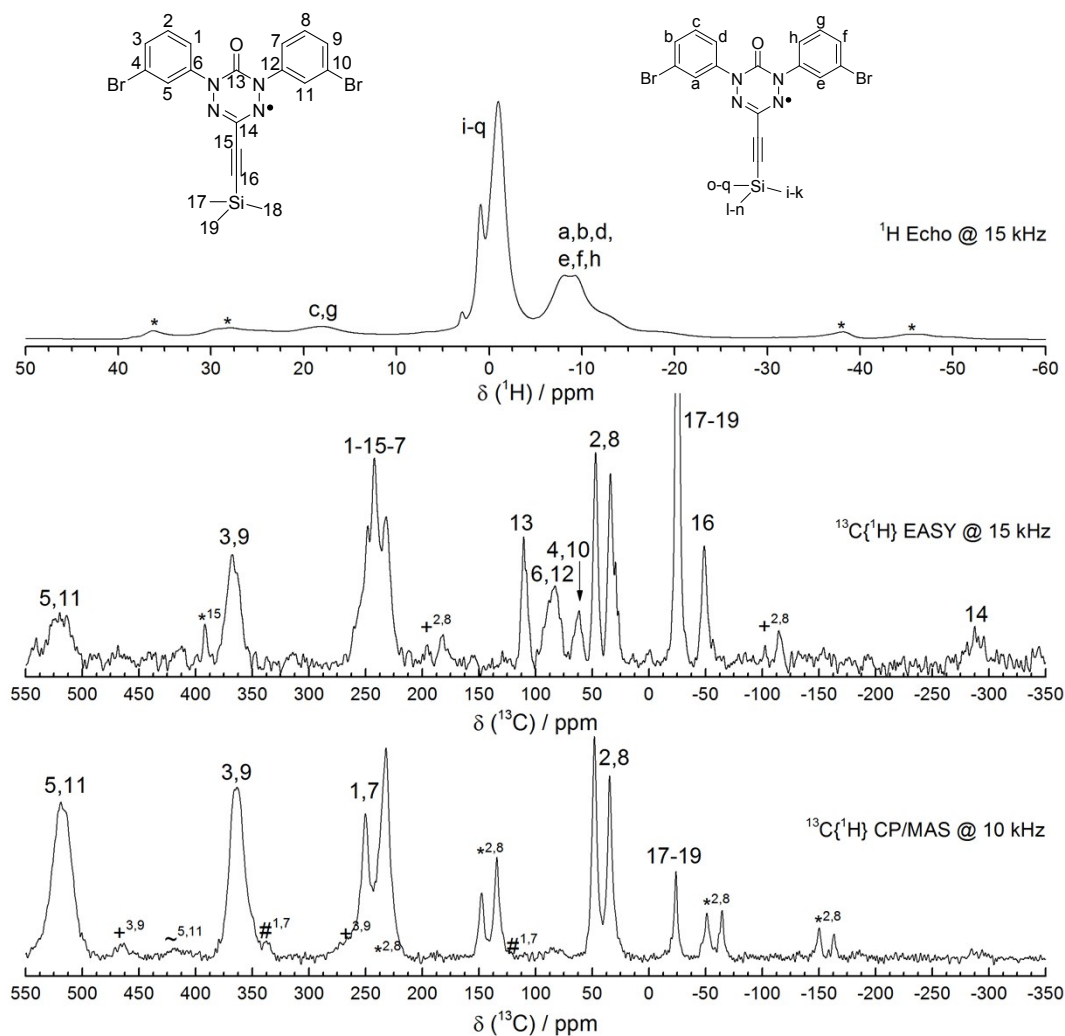
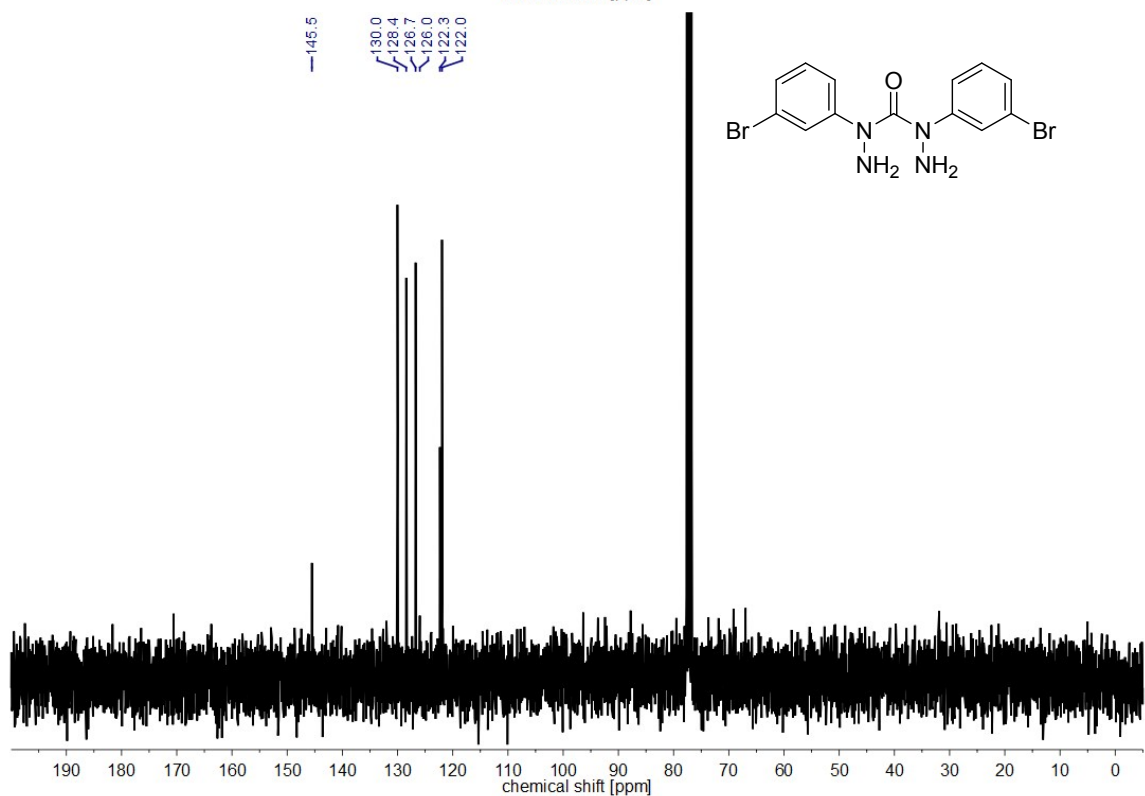
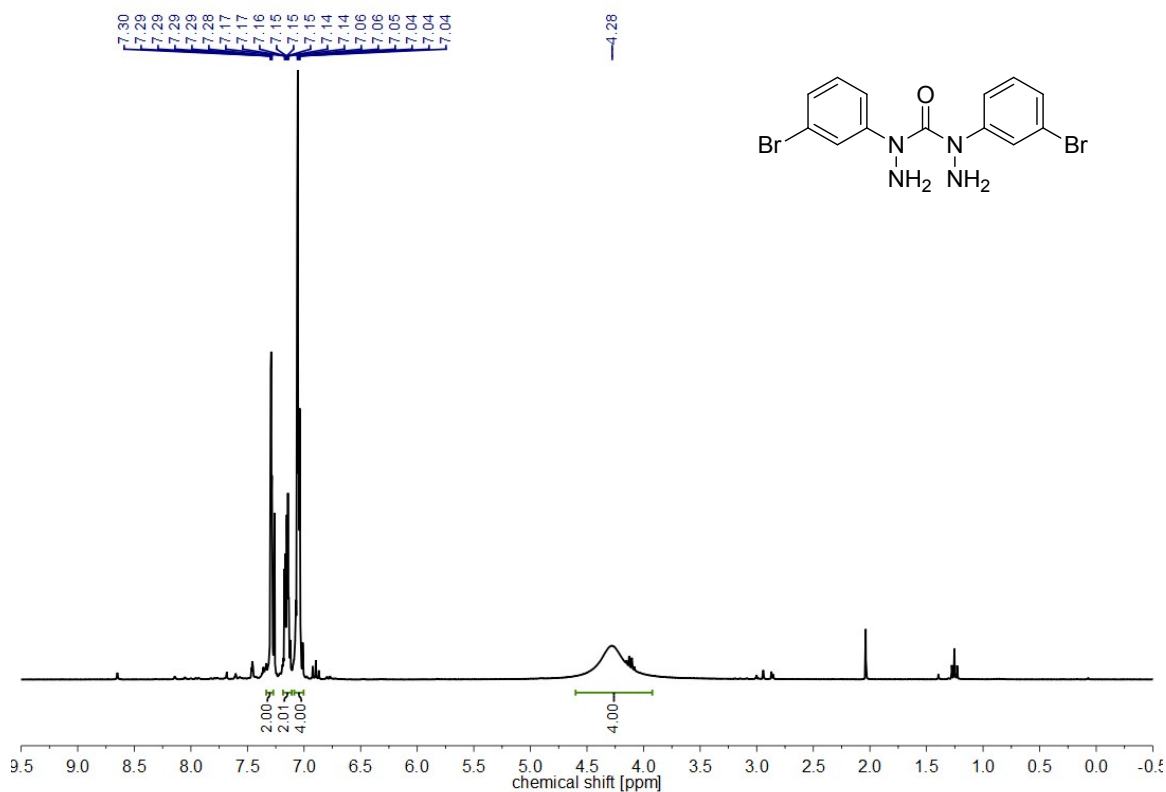


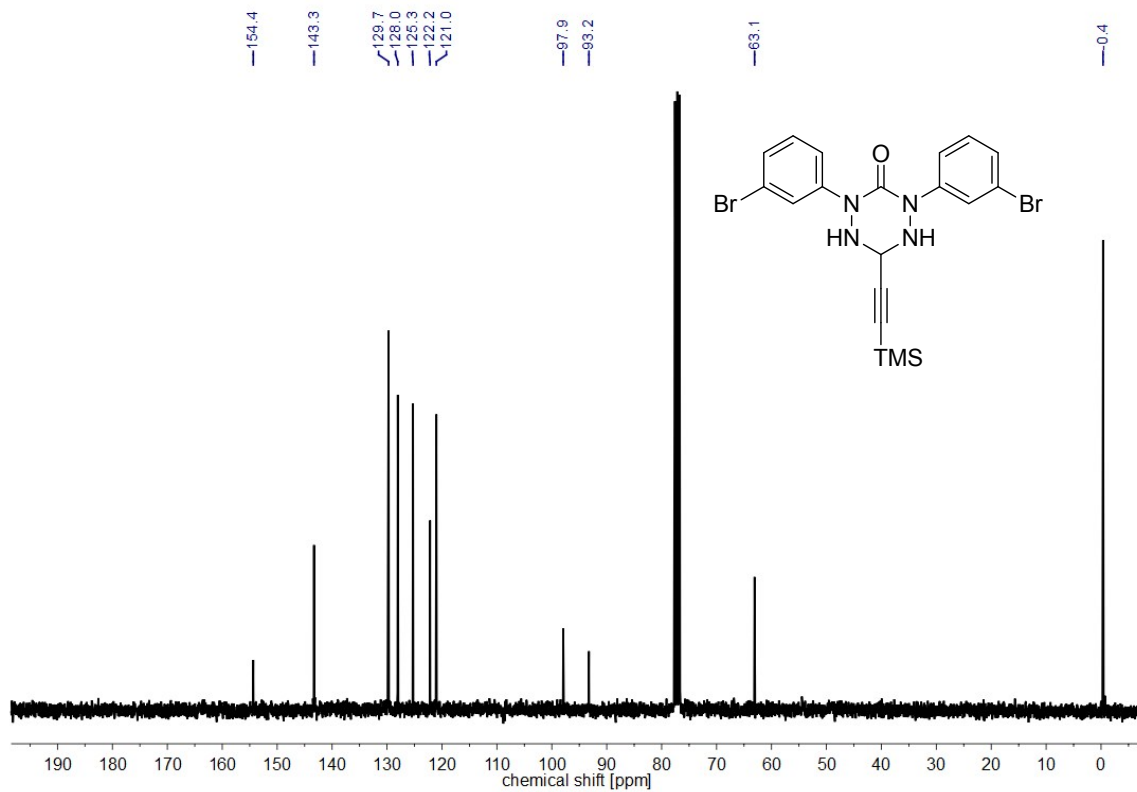
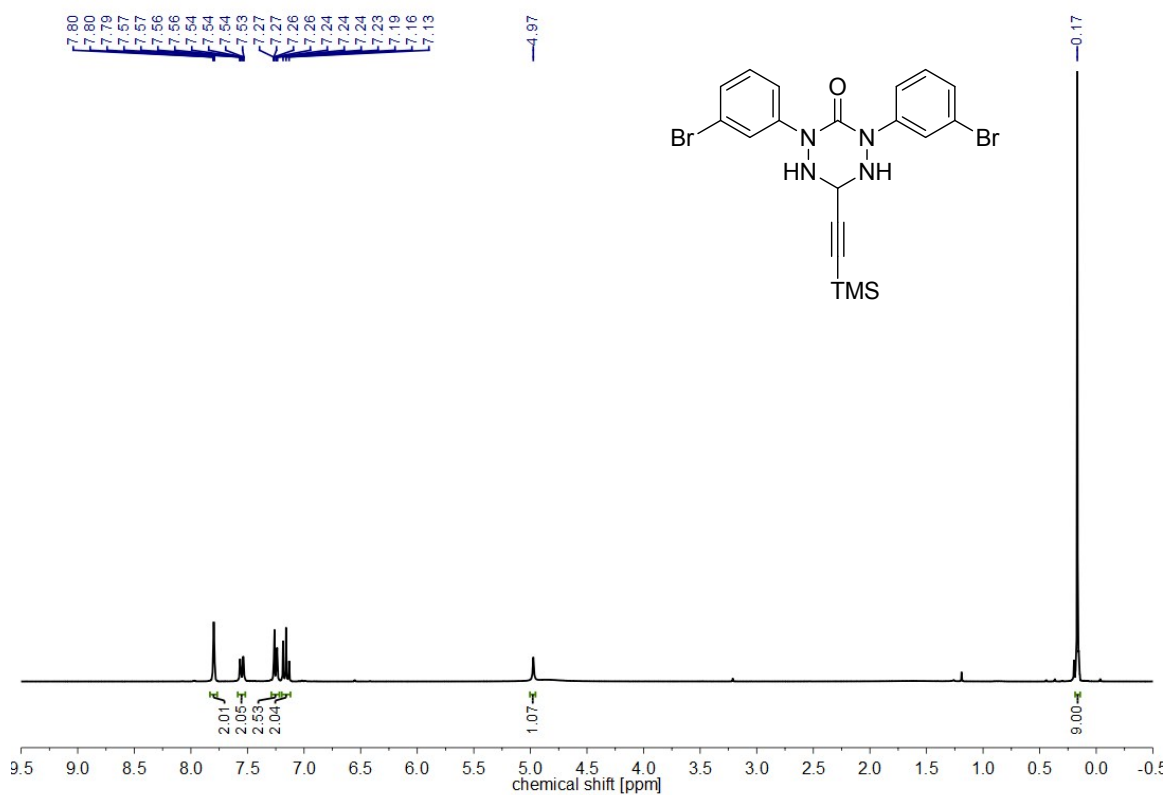
Figure S13. Solid state NMR spectra of verdazyl radical **1** with corresponding assignments: ^1H MAS-NMR spectra measured by Hahn Echo at 15 kHz (top), proton decoupled ^{13}C MAS-NMR spectra measured by the EASY pulse sequence at a rotation frequency of 15 kHz (center) and CP/MAS at 10 kHz (bottom). The bottom spectrum was measured with a short contact time of 100 μs , leading to the selective detection of protonated C-atoms.

11. ^1H and ^{13}C NMR Spectra

N,N' -Bis-(3-bromophenyl)carbonohydrazide (S1):



2,4-Bis(3-bromophenyl)-6-((trimethylsilyl)ethynyl)-1,2,4,5-tetrazinan-3-one (S2):



12. References

1. Y. Masuda, M. Kuratsu, S. Suzuki, M. Kozaki, D. Shiomi, K. Sato, T. Takui and K. Okada, *Polyhedron*, 2009, **28**, 1950-1954.
2. D. Matuschek, S. Eusterwiemann, L. Stegemann, C. Doerenkamp, B. Wibbeling, C. G. Daniliuc, N. L. Doltsinis, C. A. Strassert, H. Eckert and A. Studer, *Chem Sci*, 2015, **6**, 4712-4716.
3. Z. Otwinowski and W. Minor, *Method Enzymol*, 1997, **276**, 307-326.
4. Z. Otwinowski, D. Borek, W. Majewski and W. Minor, *Acta Crystallogr. A*, 2003, **59**, 228-234.
5. G. M. Sheldrick, *Acta Crystallogr. A*, 1990, **46**, 467-473.
6. G. M. Sheldrick, *Acta Crystallogr. A*, 2008, **64**, 112-122.
7. M. Deumal, M. J. Bearpark, J. J. Novoa and M. A. Robb, *J Phys Chem A*, 2002, **106**, 1299-1315.
8. J. J. Novoa, M. Deumal and J. Jornet-Somoza, *Chem Soc Rev*, 2011, **40**, 3182-3212.
9. L. Noodleman, *J. Chem. Phys.*, 1981, **74**, 5737-5743.
10. F. Neese, *Wires Comput Mol Sci*, 2012, **2**, 73-78.
11. C. Adamo and V. Barone, *J Chem Phys*, 1999, **110**, 6158-6170.
12. J. J. Zheng, X. F. Xu and D. G. Truhlar, *Theor Chem Acc*, 2011, **128**, 295-305.
13. C. Angeli, R. Cimiraglia, S. Evangelisti, T. Leininger and J. P. Malrieu, *J Chem Phys*, 2001, **114**, 10252-10264.
14. J. Tao, J. P. Perdew, V. N. Staroverov and G. E. Scuseria, *Phys. Rev. Lett.*, 2003, **91**, 146401.
15. F. Weigend and R. Ahlrichs, *Phys. Chem. Chem. Phys.*, 2005, **7**, 3297.
16. K. Eichkorn, O. Treutler, H. Öhm, M. Häser and R. Ahlrichs, *Chem. Phys. Lett.*, 1995, **240**, 283.
17. S. Grimme, J. Anthony, S. Ehrlich and H. Krieg, *J. Chem. Phys.*, 2010, **132**, 154104.
18. R. S. Mulliken, *J. Chem. Phys.*, 1955, **23**, 1833.
19. R. F. W. Bader, *Acc. Chem. Res.*, 1985, **18**, 9.
20. G. te Velde, F. M. Bickelhaupt, S. J. A. Baerends, C. Fonseca Guerra, J. G. Snijders and T. Ziegler, *J. Comput. Chem.*, 2001, **22**, 931.
21. E. van Lenthe and E. J. Baerends, *J. Comput. Chem.*, 2003, **24**, 1142.